NUMERICAL SIMULATIONS OF FLUID FLOW AND HEAT TRANSFER IN STRUCTURED REACTORS

A dissertation submitted in partial fulfillment

of the requirement for the award of

Bachelor of Technology in Chemical Engineering

Under the supervision and guidance of

Dr. Vivek V. Buwa

By

Anshu

2008CH10050

Department of Chemical Engineering

Indian Institute of Technology, Delhi

11 May, 2012

CERTIFICATE

This is to certify that the work presented in this report has been solely performed by me under the guidance of Dr. Vivek V. Buwa and has not been submitted by me in part or full for any other degree/diploma/certificate requirement of any other institute/organization.

Anshu

CERTIFICATE

This is to certify that the project report entitled 'Numerical Simulations of Fluid Flow & Heat Transfer in Structured Reactors' being submitted by Anshu to Department of Chemical Engineering, IIT Delhi for the award of Bachelor of Technology in Chemical Engineering is a bonafide work carried out by him under my guidance and supervision.

Dr. Vivek V. Buwa

ACKNOWLEDGEMENT

I would like to take this opportunity to thank **Dr. Vivek V. Buwa** for his guidance and support throughout the course of the project. I am grateful to him for helping me learn the fine aspects of Computational Fluid Dynamics and always guiding me towards a systematic working approach. His approach towards understanding of the problem and problem solving has been very insightful. The frequent discussions with him helped me greatly in the understanding of the minute physics aspects of the project.

I'd also want to extend my gratitude to the lab members, *Mr. V. M. Rajesh*, *Mrs. Parul Tyagi* and *Mr. Srikanth Balakrishnan* for their constant help and cooperation.

Lastly, I would thank my parents for being very motivating all the time, and my roommate, **Ms. Sonali Ranga**, who despite being an Electrical Engineer, listened to me very patiently about the infinitely many problems I faced. I also wish to express gratitude to **Mr. Ankur Goyal** for helping in my project with the learning's of his 'Summer Undergraduate Research Award' project. It'd have been impossible for me to complete this project without his constant support and encouragement.

Anshu

ABSTRACT

Computational fluid dynamic (CFD) modeling of structured reactors with realistic chemistry has been reported this work. ANSYS CFD modeling software has been used to simulate a small 'unit' monolith with implicit coupling between fluid flow, heat transfer, mass transfer, and heterogeneous chemical reactions. Steady-state calculations were performed for a catalytic methane–air combustion process with 5 reaction steps and 10 species (5 gas-phase species, 5 surface-adsorbed species). Calculations were conducted for a monolith with 57 channels discretized using 685,800 control volumes.

Keywords: Computational Fluid Dynamics, Monolith, Methane Combustion, Reacting flow

TABLE OF CONTENTS

List of tables

List of figures

Chapter 1

INTRODUCTION

A number of industrial operations involve contact between a fluid (either a gas or a liquid) and solids. In these reactors, the fluid phase contacts the solid catalyst which may be either stationary or in motion. The solid may be a catalyst or a reactant. This section will discuss the various types of catalytic reactors used industrially and their uses. Lastly the objective of the project will be defined.

1.1 Catalytic Reactors

Solid catalysts may have a homogenous catalyst or enzyme or catalytic ingredients dispersed on a support. The support may either be organic or inorganic in nature. Metal or mixed metal catalysts may be dispersed on amorphous materials (like carbon, silica or alumina), or exchanged into the cages of a zeolite. Catalysts may be shaped into monoliths, shaped pellets, spheres or powders. Some catalysts such as platinum gauzes (used for oxidation of ammonia) are in the form of several layers of fine-mesh catalyst gauza, are bulk catalysts.

Different catalysts will have different performance efficiencies which will be decided by the catalyst characteristics, internal pore structure of the support, and hence can be used in variety of reactors. The reactor selection for a particular process depends on type of catalyst chosen and its activity, selectivity, deactivation behavior, over pressure drop and heat transfer characteristics. Some types of reactors are mentioned below.

1.1.1 Wire Gauzes:

Wire screens are used for very fast catalytic reactions or reactions that require a bulk nobel metal surface for reaction and must be quenched rapidly. The nature and morphology of the gauze or the finely divided catalyst are important in reactor design. Reaction temperatures are typically very high, and residence times are of the order of milliseconds.

Examples of its application are ammonia oxidation and hydrogen cyanide synthesis using the Andrussow Process.

1.1.2 Monolith Catalyst

For fast reactions that require higher residence times, monoliths are used. Most often, monolith catalyst is an extruded ceramic honeycomb or square structure that has discrete channels that

transverse its length. The catalyst ingredients are dispersed on a high surface area support and coated on the inert monolith walls.

Monoliths may also be made of metallic supports. Stainless sheets coated with catalyst on one side can be stacked in a reactor. An extension to this design is the structured packings. Monoliths have much higher void fractions (0.65-0.91) than a packed bad, which leads to significantly lower pressure drops, and also very high geometric surface area per unit volume. The wall thickness will depend on the material of construction used and channel size varies with application.

Oval-shaped extruded cordierite or metal monolith catalysts wrapped in ceramic wool are used for emission control in automobiles. Other major uses are in Selective Catalytic Reduction of NO_x emissions from power plants and control of VOCs from chemical plants.

1.1.3 Fixed Bed

A fixed bed reactor typically is a cylindrical vessel that is uniformly packed with catalyst pellets. Nonuniform packing of catalyst pellets may cause channeling that could lead to poor heat transfer, poor conversion and catalyst deactivation due to formation of hot spots. Catalysts may be regular or shaped porous supports, uniformly impregnated with catalyst ingredient or containing a thin external shell. The size range is generally 0.1-1cm.

Heat management is an important parameter in the design of these reactors, for the reasons mentioned above. The advantage of fixed bed reactors is its easy scalability. A number of mathematical models have been developed to characterize the performance of these reactors.

Oxidation of SO_2, phosgene synthesis from CO and Cl_2 and oxidation of methanol to formaldehyde are some industrial applications of fixed beds.

1.1.4 Moving Beds

The catalyst, in the form of large granules, is circulated by gravity and gas lift between reaction and regeneration zones. The UOP platinum transformer is a major application of this concept.

Some other examples of catalytic reactors are fluidized beds, transport reactors, slurry reactors and multifunctional reactors.

1.2 Performance Analysis

For analysis of performance of these reactors, it is necessary to obtain values of pressure drop, reaction conversion, and effective heat transfer. The simplest way to do that is to perform

experiments or to analyze data available from chemical plants. But these methods will give only overall values, and will not provide information about any local variations inside the reactor. Also, the performance of these reactors will be impacted by the properties of the packings used i.e. the geometry, dimensions and material of construction used. Hence, it is necessary to study the behavior of fluid around the packings.

Hence, in this study, focus has been kept on the microscopic analysis, i.e. study of hydrodynamics and heat transfer at the scale of particle dimensions.

1.3 Objective

The objective of the present work is to do a microscopic analysis of fluid flow, heat transfer, and reaction performance in a monolith channel.

Chapter 2

LITERATURE REVIEW

The focus of this study was fixed-bed reactors, the following kinds of packings were studied for both heat transfer and reactions. This study was limited only to single-phase flows.

2.1 Spherical Packings

These are the oldest packings to be used and a significant work has been done to characterize them. Before Computational Fluid Dynamics came into use, either experiments were done, or fluid models like constant velocity (plug flow) profile were used to study fluid flow and heat transfer in fixed packed-beds. With advancements in numerical methods, focus has shifted towards the microscopic study of packed beds rather than overall properties, and 3D Navier stokes equation is solved that results in accurate solutions. This section summarizes the work done in this domain.

2.1.1 Study of Heat Transfer and Hydrodynamics

In 1980's, no definite heat transfer model was available for packed-beds. This was attributed to the complexity of the problem and experimental limitations. Models based on lumping heat transfer mechanisms and two-dimensional pseudo homogenous model were used to approximate real situations to simpler solvable conditions. Beyond this, a number of correlations have also been used to predict heat transfer parameters and pressure drop. Harris et al [1] gave a review of capabilities of CFD for Chemical Reaction Engineering

Initial studies on heat transfer in packings of spheres, using CFD, were done by Lloyd and Boehm [2]. However, these studies were limited to a 2D CFD study of a very simplified geometry. A first attempt to use a 3D CFD approach in a simple geometry of three spheres was done by Derkx and Dixon [3]. These studies were for a tube of three staggered spheres with a tube-to-particle ratio of 2.14. The problem was solved numerically by a finite element method applied to the three-dimensional incompressible Navier-Stokes equations and the energy equation. In this analysis, wall-particle contact was neglected and this led to a less realistic situation. To overcome this, Logtenberg and Dixon [4] investigated fluid flow and heat transfer at wall particle contact points to study backflow regions and increased gradients near walls.

In 2001, Dixon and Nijemeisland [5] reviewed the current state of fixed-bed reactor modeling, with an emphasis on the description of fluid flow within the bed. Challenges in the use of CFD for fixed

beds of particles were described here, and results for different tube-to-particle ratios were presented. Recently Dixon and Taskin [22] worked upon CFD studies of single sphere for high Reynolds numbers to capture vortex shedding and wake dynamics with downstream mesh refinement.

Various researchers have worked upon different particle orientations to maximize heat transfer coefficients [8, 10, 11, 18]. Yang and Nakayama [19] have performed CFD simulations on ellipsoidal particles and different packings to compare the heat transfer coefficients to that of spherical packed-beds.

Some researchers have specifically focused on pressure drops and drag coefficients. For example, Reddy and Joshi [17, 20] studied single phase pressure drop in fixed and expanded beds using CFD simulations, and studied deviations from Ergun's equation for laminar, transition and turbulent flow regimes, and wall effects on pressure drop in all regimes. Guardo et al [13] simulated Carbon dioxide in supercritical conditions. Its transport properties at high pressure were incorporated using UDF's and UDE's. They analyzed particle-to-fluid mass transfer in supercritical conditions between CO_2 and toluene, and obtained transport coefficients.

2.1.2 Reactions

In 2002, Jakobsen and Lindborg [6] tailored a numerical method for the solution of a reduced set of model equations developed for the description of reactive flows in chemical reactors. Simulations of synthesis gas and methanol production processes were performed in multi-tube fixed bed reactors.

In 2003, Dixon and Stitt [7] modeled steam reforming process in CFD simulation to incorporate the effect of reaction rate on temperature profiles in the bed. A constant wall heat flux was imposed, and spherical particles were studied with heat sinks on the surface to simulate the reforming endothermic reaction, which is mainly confined to the surface of the pellet. Local deactivation of catalyst particles leading to wall hot spots, or 'giraffe-necking' was well-reproduced by simulations.

In 2007, Dixon et al [14] improved upon the previous work of simulations of endothermic methane steam reforming reaction by including intra-particular effects (i.e. conduction, species diffusion and reaction) to result in realistic 3D flows. Catalyst Particles were taken as porous regions, with species and energy reaction sinks/sources given by UDF. Binary diffusivities were calculated from

straight-pore Knudsen and molecular diffusion coefficients, and corrected using pellet voidage and tortuosity.

In 2010, Dixon and Taskin [21] further improved the approach to CFD simulations by meshing the solid also and defining species transport and reaction inside it using UDF's. It improved upon the previous work of porous representation of the catalyst particle since imposition of convective flux across particle-fluid interface lead to inaccuracy.

2.2 Cylindrical Packings

2.2.1 Hydrodynamic Study

Motlagh and Hashemabadi [15] studied heat transfer characteristics of solid cylinders in a bed with tube-to-particle diameter ratio equal to 2, by the presence of contact points between the cylinders using κ-ε turbulence models. From mass and heat transfer analogy, the Nusselt numbers for each cylindrical particle in bed were found from the corresponding Sherwood numbers. Mothlag and Hashemabadi [16] also did two- and three-dimensional CFD modeling of heat transfer from cylindrical particles in different configurations including infinite cylinder in cross-flow, cross-flow on finite cylinder with different aspect ratio in a rectangular duct, axial-flow on finite cylinder and axial-flow on finite cylinder with upstream turbulence.

2.2.2 Reactions

Dixon and Stitt [9] compared heat transfer performance of cylindrical particles with varying number of internal voids in a steam reforming packed-bed-reactor tube.

Kolaczkowski and Chao [12] used CFD to model catalytic combustion of propane in a fixed bed with spherical and cylindrical pellets. The coupled processes of diffusion and chemical reaction, combined with heat and mass transfer effects were modeled in a catalyst pellet.

In 2010, Dixon et al [22] used the advanced technique of modeling species transport and reaction inside cylindrical catalyst particles also to obtain realistic concentration and temperature profiles.

2.3 Structured Packings

Structured packing is a recent advancement in chemical industries. The use of structured packings was primarily limited to reactive distillation only, and a lot of experimental data is available for them for different packing geometries. With developments in CFD, different packing geometries

with inbuilt corrugations and intrusions are being modeled to obtain maximum HETP and least pressure drop possible.

The classical way of determination of dry pressure drop was to use Ergun's equation with experimental data fitting to calculate constants for a given packing. This method provided no flexibility with respect to corrugation angle, channel size or packing topography.

Some research that has been done on a unit cell of structured packing to study the fluid flow over packing sheet has been discussed here. Valluri et al [23] developed a mathematical model of film flow for moderate Reynolds numbers (~30) and compared them to results obtained from CFD, to study film wave growth on corrugations of Mellapak® packings and to calculate film interfacial area, also predicting the effect of packing geometry on flow characteristics. Szulczewska and Gorak [34] studied liquid flow on films of Mellapak 250Y to determine the minimum liquid flow rate for an unbroken liquid film at packing surface. Gu et al [25] used VOF method to hydrodynamics of falling film flow on inclined plane resulting from gas-liquid interactions. The role of material properties such as viscosity, surface tension, liquid film thickness, flow direction was discussed in determination of mass transfer efficiency and pressure drop.

Petre et al [24] developed a combined mesoscale-microscale predictive approach to apprehend the aerodynamic macroscale phenomena in structured packings. It identified recurrent mesoscale patterns wherein the constitutive microscale dissipation mechanisms occur. Each mechanism was simulated over complete range of Reynolds number, using 3D CFD, and overall pressure drop was reconstructed. To validate, these results were compared against five different Sulzer packings. Mahr and Mewes [30] also modeled macroscopic gas–liquid two-phase flow field of an entire column to study effects like large scale maldistribution and instabilities in the flow field. The model was based on elementary cell model, and extended to be used on anisotropic porous structures.

Said et al [26] developed correlations for dry pressure drop and channel height dimension, channel opening angle and corrugation angle in a structured packings using CFD, focusing on pressure loss friction component. Said et al [26] and Nikou and Ehsani [27] also compared the results obtained by different turbulence models available in CFD packages. Fernandez et al [28,29] also performed a similar study on supercritical fluids to understand influence of shape and geometry on hydrodynamics for dry and wet pressure drop calculations for both laminar and turbulent flow regimes using Sulzer EX gauze packing. Zivdar et al [31] also did dry pressure drop simulations for

Katapak-S in turbulent flow regime and studied flow regimes for dead zones and internal circulation zones.

Significant work has also been carried out to calculate distillation efficiencies of different structured packings, where new packing geometries have been developed with higher performance [32, 33]. Since reactive distillation has already been studied in detail, this part has not been covered in the present study.

2.4 Monoliths

This part of the study was aimed at finding out the various types of gas-phase reactions that are been industrially carried out in monolithic reactors, or have a potential application.

There are many research works that have been done assuming the single channel model i.e. no coupling of heat transfer b/w adjacent channels is assumed. Liu et al [35] developed a novel design of a single channel monolith for surface reaction with enhanced mass transfer. Catalytic combustion of methane (with air as the oxidizing species) with first order kinetics was selected as the model reaction, and the reaction was modeled in the porous region and on the solid wall. Canu and Vecchi [37] also studied the same reaction system for single channel only. Benedetto et al [36] studied catalytic propane combustion, in a single channel monolith, with coupling of fluid flow on mass and energy fluxes. The reaction is assumed to occur only at the reaction surface, and hence correlations of Nusselt number and Sherwood number have been developed for reaction zone. In the same study, Donsi et al [38] analyzed the impact of increasing Re on heat and mass transfer resulting from high axial diffusions. 2D and 3D single channel monolith models have been developed for NO_x absorption into a NaZSM-5 catalyst film by Perdana et al [40]. Cordierite has been used as the monolith material, and the factors influencing the reaction conversion have been analyzed numerically. Lei et al [42] also use 3D CFD models to analyze the performance of NO removal in monolithic honeycomb catalytic reactors. Many more researches along with these suggest that *single channel models* have been used most frequently to model the *surface reaction* of *hydrocarbon reforming*.

Mei et al [39] developed a catalyst coated metal monolith used inside a double pipe heat exchanger and improved reactor performance by varying catalyst coating methods and channel arrangements. Chen and Yang [41] presents a review of the state of the art techniques that have been used in monolith modeling: both numerically and using simulations.

Mazumdar et al [43, 44, 45] has presented work on effect of heat transfer coupling in channels. [45] also presents the impact of channel length on reaction conversion and efficiency.

Chapter 3

COMPUTATIONAL MODEL

3.1 Governing Equations

3.1.1 The Mass Conservation Equation

The equation for conservation of mass, or continuity equation, can be written as follows:

$$\frac{\partial \rho}{\partial t} + \nabla \cdot (\rho \vec{v}) = S_m \qquad \text{... (01)}$$

This is the general form of the mass conservation equation and is valid for incompressible as well as compressible flows. The source S_m is the mass added to the continuous phase from the dispersed second phase (e.g., due to vaporization of liquid droplets) and any user-defined sources.

3.1.2 Momentum Conservation Equations

Conservation of momentum in an inertial (non-accelerating) reference frame is described as:

$$\frac{\partial}{\partial t}(\rho \vec{v}) + \nabla \cdot (\rho \vec{v} \vec{v}) = -\nabla p + \nabla \cdot (\bar{\bar{\tau}}) + \rho \vec{g} + \vec{F} \qquad \text{... (02)}$$

where p is the static pressure, $\bar{\bar{\tau}}$ is the stress tensor (described below), and $\rho \vec{g}$ and $\vec{F}$ are the gravitational body force and external body forces (e.g., that arise from interaction with the dispersed phase), respectively. F also contains other model-dependent source terms such as porous-media and user-defined sources.

The stress tensor $\bar{\bar{\tau}}$ is given by

$$\bar{\bar{\tau}} = \mu \left[(\nabla \vec{v} + \nabla \vec{v}^{\,\mathrm{T}}) - \frac{2}{3} \nabla \cdot \vec{v} I \right] \qquad \text{... (03)}$$

where μ is the molecular viscosity, I is the unit tensor, and the second term on the right hand side is the effect of volume dilation.

3.1.3 The Energy Equation

The energy equation in the following form:

$$\frac{\partial}{\partial t}(\rho E) + \nabla \cdot (\vec{v}(\rho E + p)) = \nabla \cdot \left(k_{\text{eff}} \nabla T - \sum_j h_j \vec{J}_j + (\bar{\bar{\tau}}_{\text{eff}} \cdot \vec{v}) \right) + S_h \qquad \text{... (04)}$$

where k_{eff} is the effective conductivity ($k + k_t$, where k_t is the turbulent thermal conductivity, defined according to the turbulence model being used), and J_j is the diffusion flux of species j. The first three terms on the right-hand side of the equation represent energy transfer due to conduction, species diffusion, and viscous dissipation, respectively. S_h includes the heat of chemical reaction, and any other volumetric heat sources. Also,

$$E = h - \frac{p}{\rho} + \frac{v^2}{2} \qquad \text{... (05)}$$

where h is the sensible heat enthalpy defined as

$$h = \sum_j Y_j h_j \qquad \text{... (06)}$$

for an ideal gas and

$$h = \sum_j Y_j h_j + \frac{p}{\rho} \qquad \text{... (07)}$$

for incompressible flows. In both these equations, Y_j is the mass fraction of species j, and h_j is calculated as:

$$h_j = \int_{T_{\text{ref}}}^{T} c_{p,j}\, dT \qquad \text{... (08)}$$

where T_{ref} is 298.15 K.

Sources of energy, S_h, include the source of energy due to chemical reaction:

$$S_{h,\text{rxn}} = -\sum_j \frac{h_j^0}{M_j} \mathcal{R}_j \qquad \text{... (09)}$$

where h_j^0 is the enthalpy of formation of species *j* and R_j is the volumetric rate of creation of species *j*.

3.1.3-1 Energy Equation in Solid Region

In solid regions, the energy transport equation used has the following form:

$$\frac{\partial}{\partial t}(\rho h) + \nabla \cdot (\vec{v}\rho h) = \nabla \cdot (k\nabla T) + S_h \quad \text{... (10)}$$

Where ρ = density,

h = sensible enthalpy,

k = conductivity,

T = temperature,

S_h = volumetric heat source

The second term on the left-hand side represents convective energy transfer due to rotational or translational motion of the solids. The velocity field $\vec{v}$ is computed from the motion specified for the solid zone. The terms on the right-hand side are the heat flux due to conduction and volumetric heat sources within the solid, respectively.

3.1.4 The Species Transport Equation

The convection-diffusion equation for chemical species is

$$\frac{\partial}{\partial t}(\rho Y_i) + \nabla \cdot (\rho \vec{v} Y_i) = -\nabla \cdot \vec{J}_i + R_i + S_i \quad \text{... (11)}$$

Where Y_i is the mass fraction of species *i,* R_i is the net rate of production of species i by chemical reaction, and S_i is the rate of creation by addition from the dispersed phase plus any user-defined sources. This equation will be solved for *N-1* species where *N* is the total number of fluid phase chemical species present in the system. Since the mass fraction of the species must sum to unity, the N^{th} mass fraction is determined as one minus the sum of the *N-1* solved mass fractions. To minimize numerical error, the N^{th} species should be selected as that species with the overall largest mass fraction.

3.2. Geometrical Model, Boundary Conditions & Solution Domain

3.2.1 Geometrical Model

In the present work, a monolith has been considered with the following dimensions.

ID = 17.6 mm

OD = 18.4 mm

Length = 1000 mm

Wall thickness = 0.4 mm

Channel dimensions = 1.6 mm x 1.6 mm

A total of 57 channels were made

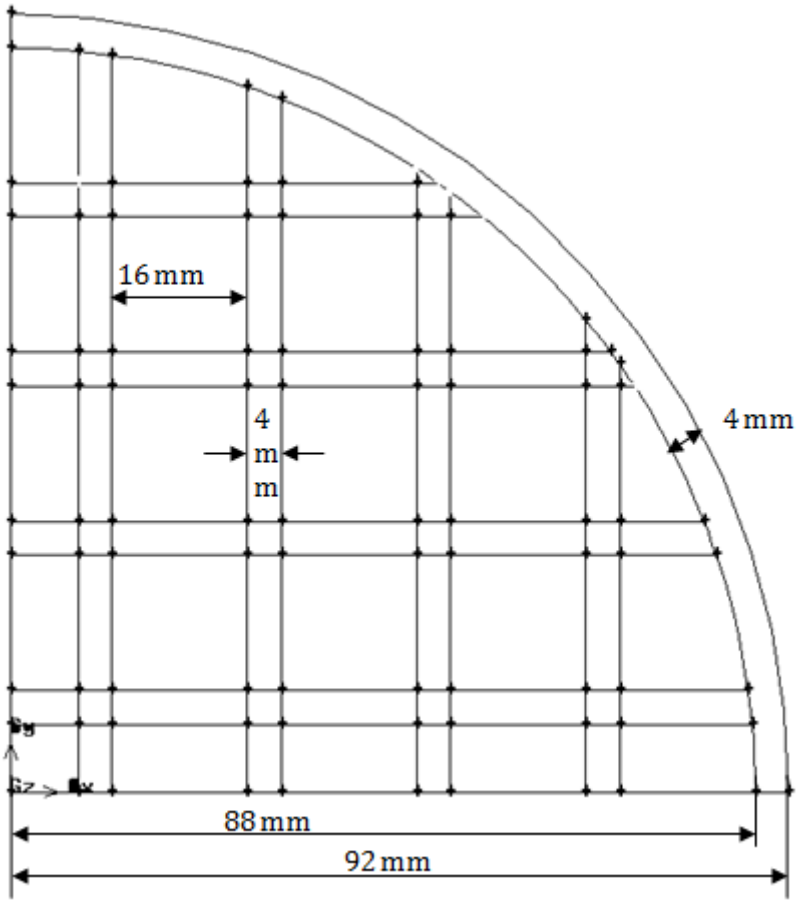

Figure 3.1: Cross Section of geometry

The material for monoliths is taken to be cordierite, as used industrially. Material properties have been taken from Lynch [46].

Density = 2511 kg/m^3

C_p = 1046 J/kg-K

Thermal Conductivity = 3 W/m-K

Mesh size was taken to be 0.1mm and faces were meshed using 'Quad' elements and 'Map' and 'Pave' type. Volume mesh was created using 'Hex/Wedge' elements and 'Cooper' type, which resulted in 685800 cells, 2188158 faces and 813671 nodes. The geometry mesh was created in Gambit 2.4.6, and all simulations were performed in Fluent 6.3.26.

NOTE: The grid density was used as mentioned in [43]; hence grid independence check was not performed.

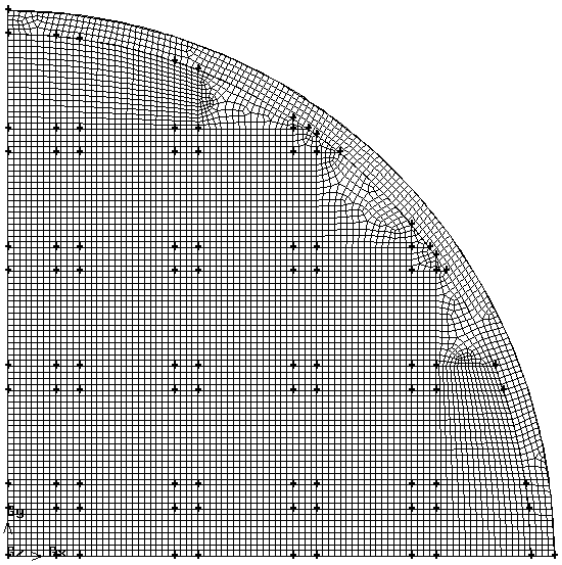

Figure 3.2: Cross Section of geometry with mesh visible

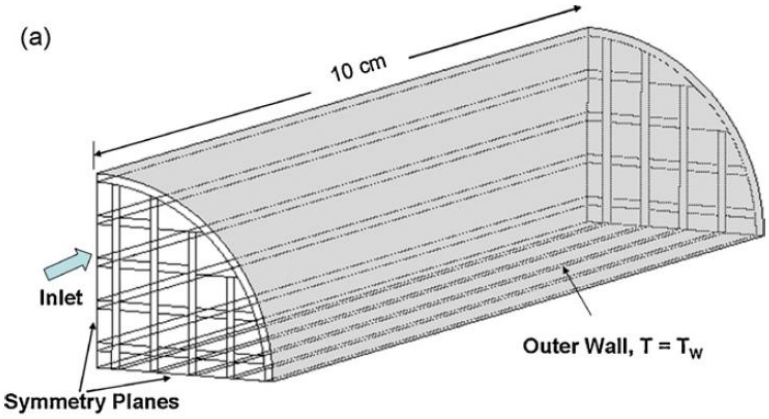

Figure 3.3: Isometric View of Geometry, Boundary Conditions

3.2.2 Boundary Conditions

The monolith was divided by two perpendicular diameters and only one-fourth of the monolith was modeled. The boundary conditions used are mentioned in Table-1.

Table 3.1: Boundary Conditions

Face	**Boundary Condition**
Flow entry	Velocity Inlet
Flow exit	Outflow
Channel walls	Wall
Symmetry planes	Symmetry

NOTE: While modeling this geometry, bottom-up approach was used; this means that first vertices, then edges, then faces, and then volumes were created. This was done so as to ensure than no extra face or edge is being created. This is a necessary condition for the modeling of heat transfer. When such geometry is imported in Fluent, the walls which are bounded by two different materials develop a wall: shadow as another zone. Auto-generation of wall: shadow zone is mandatory for heat transfer across that wall. In case any extra face is present, this wall: shadow will not be created and coupled heat transfer will not occur across the wall. (Instead a B.C. will have to be defined like constant wall flux or temperature, which will result in simulation errors.)

3.2.3 Discretization and Solution

A 3D steady-state pressure based solver was used. SIMPLE Pressure-Velocity Coupling was used. The simulations were started with the default Discretization schemes and under-relaxation factors, as mentioned in the table below.

Table 3.2: Initial Control Parameters

Under-relaxation factors		**Discretization**	
Pressure	0.3	Pressure	Standard
Density	1	Momentum	First Order Upwind
Body Forces	1	CH_4	First Order Upwind
Momentum	0.7	O_2	First Order Upwind
CH_4	1	CO	First Order Upwind
O_2	1	H_2	First Order Upwind
CO	1	Energy	First Order Upwind
H_2	1		
energy	1		

Since the number of nodes was 0.8 million, and each node had 9 variables, a total of 7.2 million variables were reported in every iteration, which led to very complex and unstable iterations. Hence the Discretization schemes and under-relaxation factors were kept at default initially, and as iterations proceeded, these values were reduced in steps. The final data that was obtained was obtained after convergence was attained at the following values. Convergence criteria are mentioned in Table-4.

Table 3.3: Final Control Parameters

Under-relaxation factors		**Discretization**	
Pressure	0.1	Pressure	Standard
Density	0.3	Momentum	QUICK
Body Forces	0.3	CH_4	Second Order Upwind
Momentum	0.2	O_2	Second Order Upwind
CH_4	0.3	CO	Second Order Upwind
O_2	0.3	H_2	Second Order Upwind
CO	0.3	Energy	QUICK
H_2	0.3		
energy	0.2		

Table 3.4: Residuals

Residual	**Absolute Criteria**
Continuity	1e-04
x-velocity	1e-05
y-velocity	1e-05
z-velocity	1e-05
Energy	1e-06
CH_4	0.001
O_2	0.001
CO	0.001
H_2	0.001

Chapter 4

RESULTS AND DISCUSSIONS

4.1 Base Case Simulations

4.1.1 Fluid Flow

For fluid flow simulations, a mixture of methane and air was taken. Reynolds number was taken to be 130 [43], hence inlet velocity = 0.9m/s. Graphs of velocity magnitude against curve length are plotted below.

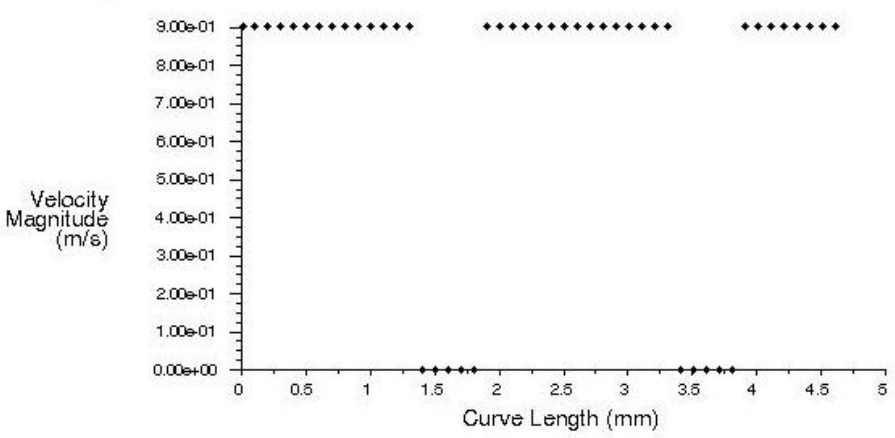

Figure 4.01: Velocity along diameter at inlet

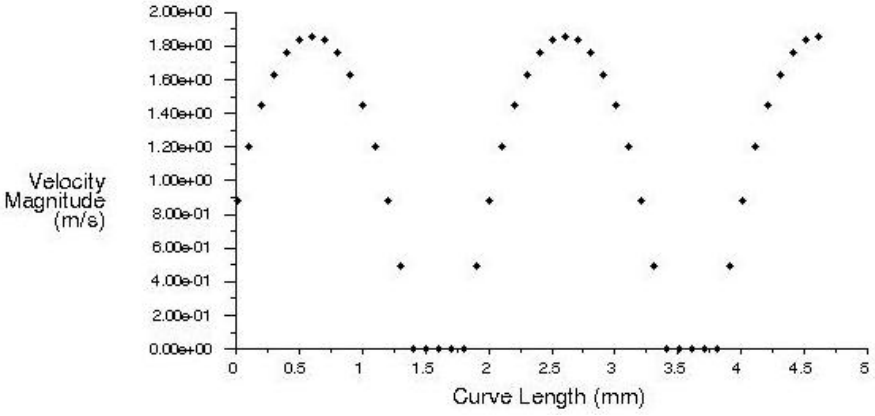

Figure 4.02: Velocity along diameter at outlet

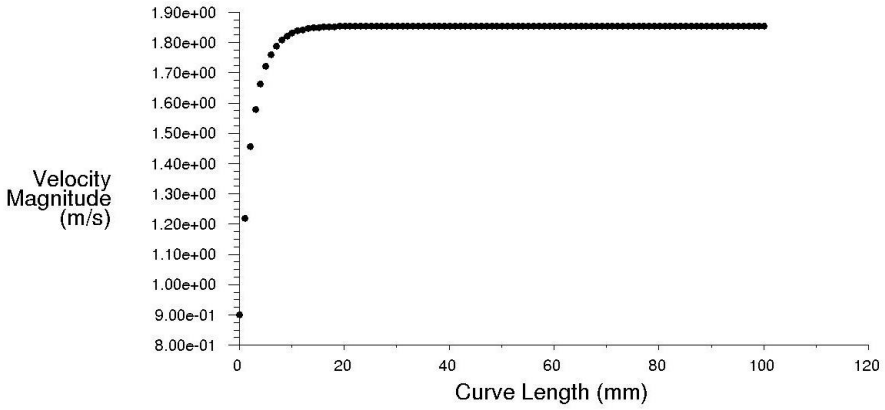

Figure 4.03 Velocity along centerline

Figure 4.1 is the velocity profile at inlet. Figure 4.2 clearly indicates parabolic velocity profile in each channel, as expected for analytical results. Figure 4.3 shows that the velocity profile was fully developed before z=20mm only. Figure 4.4 represents contours of velocity perpendicular to centerline.

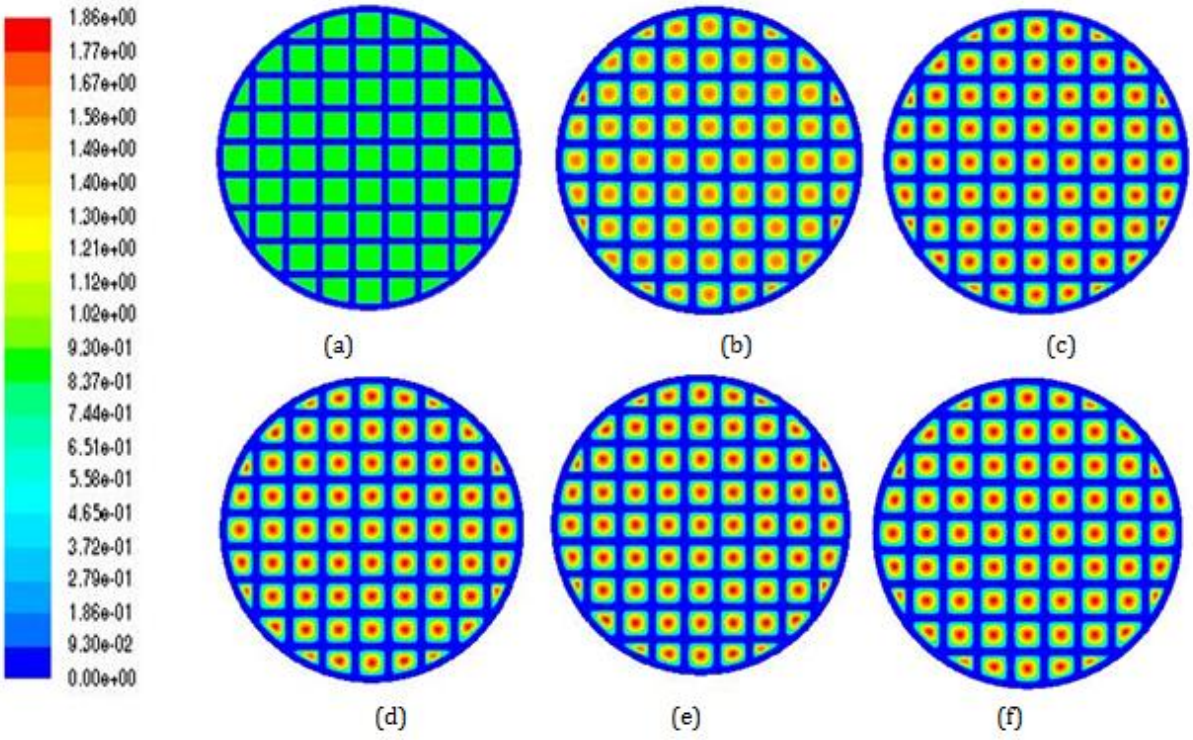

Figure 4.04: Contours of velocity at cross sections of monolith at
(a) z = 0mm, (b) z = 5mm, (c) z = 10mm, (d) z = 15mm, (e) z = 20mm & (f) z = 25mm.

4.1.2 Heat Transfer

Inlet flow was kept at 400°C and outer wall of the monolith was kept at 1300°C. Graphs of static temperature against curve length are plotted below. Figure 4.6 represents temperature contours along the length of the monolith, on a plane passing through the centre. Figure 4.7 represents temperature contours along the cross section of the monolith

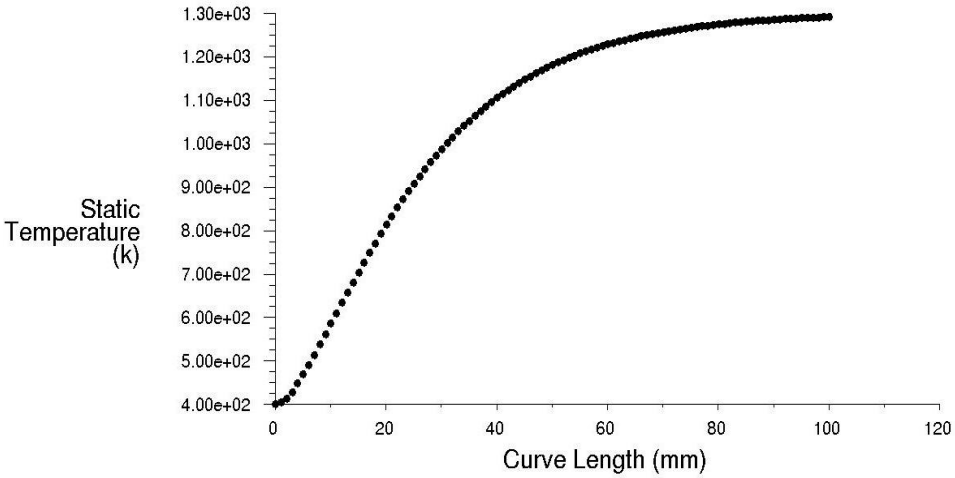

Figure 4.05: Temperature along centerline

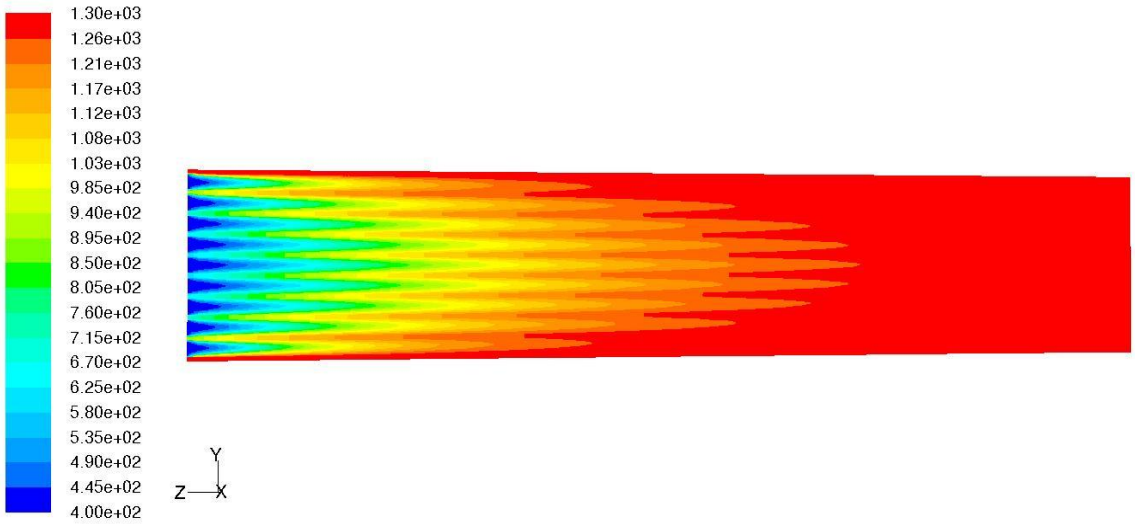

Figure 4.06: Temperature contour along the length of monolith

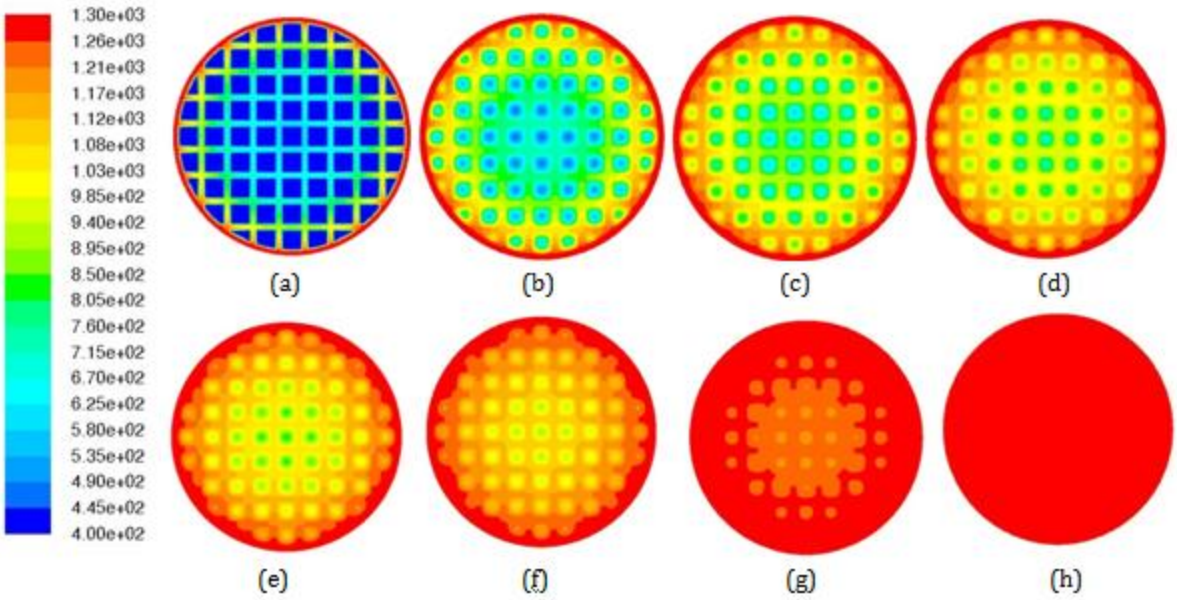

Figure 4.07: Contours of temperature at cross sections of monolith at (a) z = 0mm, (b) z = 5mm, (c) z = 10mm, (d) z = 15mm, (e) z = 20mm, (f) z = 25mm, (g) z = 50mm & (f) z = 75mm.

4.2 Volumetric Reaction

Monolithic reactors work very well in cases where pressure drop is to be reduced and heat generated has to be carried away. Also, monoliths works best for mass transfer limited cases, where diffusion rates are much higher than the reaction rate, i.e. η is very low.

One such industrial application of monoliths is steam reforming of bio-oils. So, in the present case, we will start with steam reforming of methane to produce hydrogen.

The present reaction kinetics consider three parallel reactions as follows

$$CH_4 + H_20 \Leftrightarrow CO + 3H_2 \quad (1)$$

$$CO + H_20 \Leftrightarrow CO_2 + H_2 \quad (2)$$

$$CH_4 + 2H_20 \Leftrightarrow CO_2 + 4H_2 \quad (3)$$

The expressions for the reaction rates are as follows:

$$R_1 = (k_1/p_{H2}^{2.5})*(p_{CH4}p_{H20} - p_{H2}^3 p_{CO}/K_1)/Den^2$$

$$R_2 = (k_2/p_{H2})*(p_{CO}p_{H20} - p_{H2}p_{CO2}/K_2)/Den^2$$

$$R_3 = (k_3/p_{H2}^{2.5})*(p_{CH4}p_{H20}^2 - p_{H2}^3 p_{CO2}/K_1K2)/Den^2$$

$$Den = 1 + K_{CO}P_{CO} + K_{H2}P_{H2} + K_{CH4}P_{CH4} + K_{H2O}P_{H2O}/P_{H2}$$

The reaction rate parameters, taken from [47], are as follows:

$K_1 = 10266.76 * e^{-26830/T+30.114}$

$K_2 = e^{4400/T-4.036}$

$k_1 = 9.49 * 10^{16} * e^{-240100/RT}$

$k_2 = 4.39 * 10^{4} * e^{-67130/RT}$

$k_3 = 2.29 * 10^{16} * e^{-243900/RT}$

$k_{CH4} = 6.65 * 10^{-6} * e^{38280/RT}$

$k_{CO} = 8.23 * 10^{-7} * e^{70650/RT}$

$k_{H20} = 1.77 * 10^{5} * e^{-88680/RT}$

$k_{H2} = 8.23 * 10^{-22} * e^{82900/RT}$

The above reactions and parameters were added to Fluent using User Defined Functions.

The UDF was compiled and hooked up successfully in Fluent 6.3 but iterations using the UDF gave the following errors:

1. Reversed flow in 14 faces on pressure-outlet 5.
2. temperature limited to 3.990000e+002 in 54400 cells on zone 2 in domain 1
3. temperature limited to 3.990000e+002 in 51200 cells on zone 3 in domain 1
4. Concentration of hydrogen is coming out to be zero at the end of second iteration, even though there is no source of consumption of hydrogen. This might be because of some unrealistic source being generated.

All these errors converged to resolving of the error shown in Figure 4.8.

```
  iter continuity x-velocity y-velocity z-velocity     energy        ch4        h2o          co     time/iter
!   52 solution is converged
    52 6.6003e-06 2.2792e-08 2.2780e-08 8.9899e-06 5.8316e-11 1.3433e-16 1.3549e-16 0.0000e+00  0:00:00    5
 temperature limited to 1.000000e+000 in 118204 cells on zone 2 in domain 1
  temperature limited to 1.000000e+000 in 298622 cells on zone 4 in domain 1
     53 5.8270e-06 2.0270e-08 2.0266e-08 7.9125e-06 5.3687e-04 3.2759e-11 7.4190e-02 1.3460e-03  0:29:44    4
    54 6.0304e+02 1.8050e-08 1.8047e-08 6.9749e-06 1.#QNBe+00 1.#QNBe+00 1.#QNBe+00 1.#QNBe+00  0:22:10    3

 reversed flow in 2011 faces on pressure-outlet 10.
    55 1.#QNBe+00 1.5115e-03 1.5293e-03 2.1854e-02 1.#QNBe+00 1.#QNBe+00 1.#QNBe+00 1.#QNBe+00  0:14:34    2
```

Figure 4.08: Snapshot of 'Temperature limitation' error

The temperature was getting limited to either the minimum or the maximum defined value in almost all cases. This error keeps on repeating even for the simplest possible geometry (smallest

possible mesh size) and for the predefined reaction of methane-air combustion in Fluent, for different combinations of solution schemes.

This leads to a conclusion that the problem is not with the present problem or the geometry or the solution conditions, but it is a problem with the Fluent package in solution of high temperature reactions with Arrhenius rate law governing. The solution complexity was very high, and even with the cluster processors, no convincible solution could be obtained. Hence we were unable to model high temperature volumetric reactions in monoliths using Fluent. Hence, we tried modeling surface reactions which was a more realistic case in case of catalyst coated monoliths.

4.3 Surface Reactions

To model surface reactions, Mazumdar [43] used reaction mechanisms as used by Raja [50]. Reaction mechanisms for methane combustion using oxygen on a Pt surface were developed using Langmuir Hinshelwood Haugen Watson model, which involved 24 heterogeneous reactions, involving seven gas phase species, and 11 surface-absorbed species. As a conclusion, Mazumdar [43] also mentioned that the final conversion does not vary much with changes in surface reaction mechanisms. Some main reactions are the major influencing factors. Hence, due to limitations of the solver and the processor, two different mechanisms were taken into consideration in the present study: a II-step mechanism, and a V-step mechanism.

4.3.1 II-step reaction mechanism

An inlet mixture of methane, oxygen and nitrogen (mass fractions: 0.4:0.3:0.3) was taken, keeping all other parameters as mentioned earlier. The following reaction was considered

$$CH_4 + 0.5\ O_2 \rightarrow CO + 2\ H_2$$

The following reaction mechanism was considered.

1. $CH_4 + Pt(s) \rightarrow C(s) + 2\ H_2$
2. $0.5\ O_2 + C(s) \rightarrow CO + Pt(s)$

The reaction parameters and species properties, as obtained from [48], are mentioned in Table 4.1.

Table 4.1: Reaction rate parameters for II-step reaction mechanism

	Reaction 1	**Reaction 2**
Pre Exponential Factor	1e+6	1e+12
Temperature Exponent	0.5	0.5
Activation Energy	0	0
Rate	$k[CH_4][Pt(s)]$	$k[O_2][C(s)]$

The properties of site species and gas phase species were picked up from Fluent tutorials [48] and Fluent database respectively.

The average for CH_4 molar concentration (kgmol/m^3) at inlet and outlet has been computed.

```
--------------------------------- --------------------
                  flow_in         0.011883
                 flow_out         0.001356
          ---------------- --------------------
                      Net         0.010527
```

Hence, Conversion (wrt CH4) = 0.885903

4.3.2 V-step reaction mechanism

Again, an inlet mixture of methane, oxygen and nitrogen (mass fractions: 0.4:0.3:0.3) was taken, keeping all other parameters as mentioned earlier. The following reaction was considered

$$CH_4 + 0.5\ O_2 \rightarrow CO + 2\ H_2$$

The following reaction mechanism was considered.

1. $CH_4 + 5Pt(s) \rightarrow C(s) + 4H(s)\ 2\ H_2$
2. $O_2 + 2Pt(s) \rightarrow 2O(s)$
3. $C(s) + O(s) \rightarrow CO(s) + Pt(s)$
4. $CO(s) \rightarrow CO + Pt(s)$
5. $2H(s) \rightarrow Pt(s) + H_2$

The reaction parameters, as obtained from [50], are mentioned in Table 4.2.

Table 4.2: Reaction rate parameters for V-step reaction mechanism

Reaction	**1**	**2**	**3**	**4**	**5**
Pre Exponential Factor	2.60E+05	1.80E+05	3.70E+05	1.00E+09	3.70E+07
Temperature Exponent	0.5	0.5	0	0	-0.5
Activation Energy (j/mol)	0	0	6.28E+04	1.26E+05	6.74E+04
Rate	$k[CH_4][Pt(s)]^{2.3}$	$k[Pt(s)]$	$k[C(s)][Pt(s)]$	$k[CO(s)]$	$k[H(s)]$

The properties of site species and gas phase species were picked up from Fluent tutorials [48] and Fluent database respectively. The results obtained have been shown in the following figures.

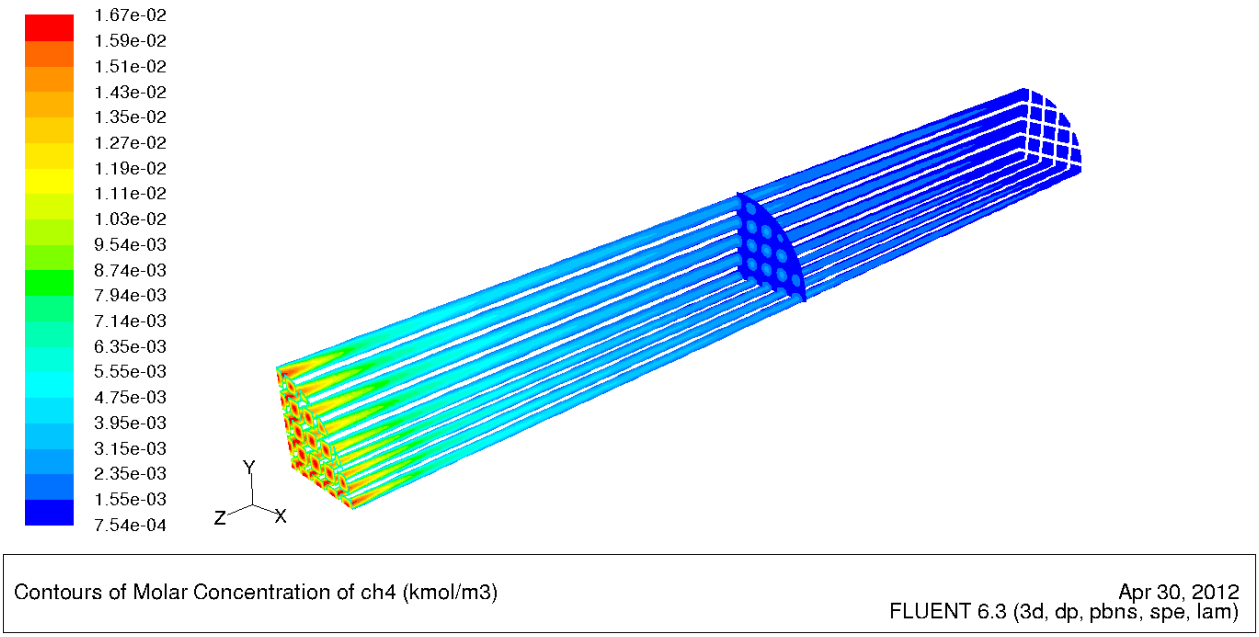

Figure 4.09: Contours of molar concentration of CH_4 along the length of monolith

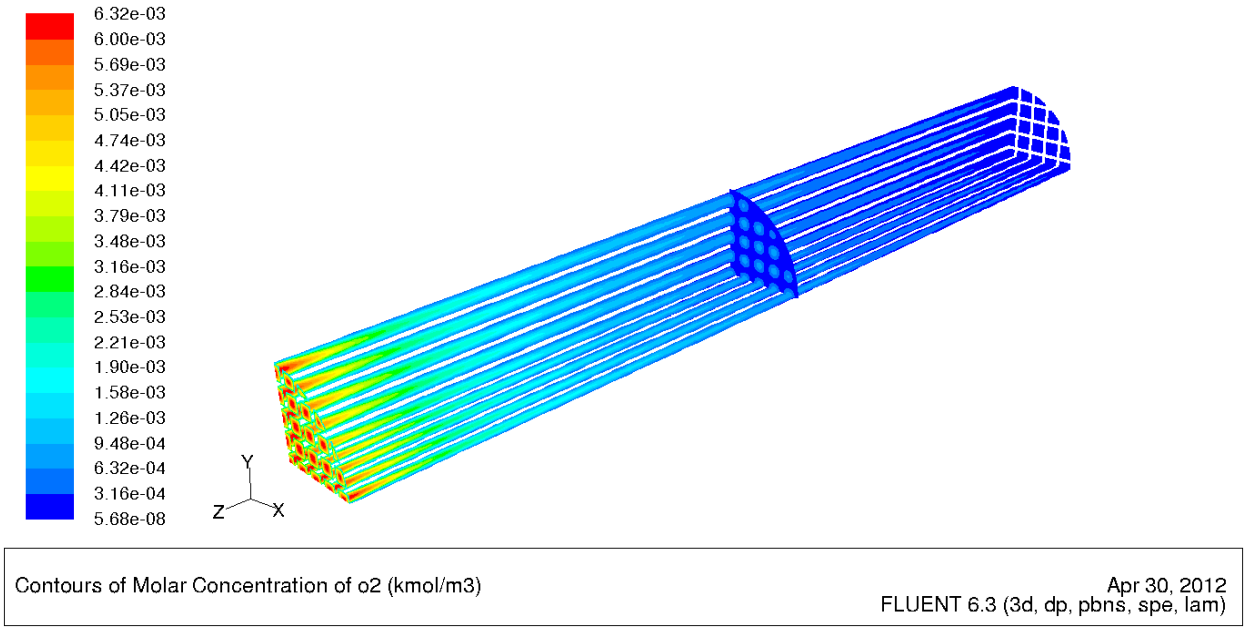

Figure 4.10: Contours of molar concentration of O_2 along the length of monolith.

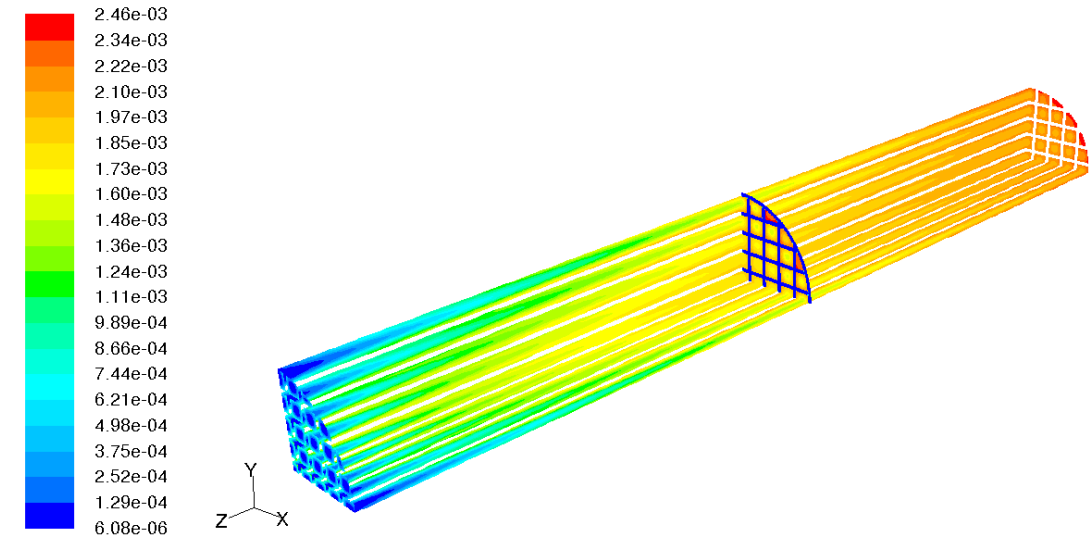

Figure 4.11: Contours of molar concentration of CO along the length of monolith.

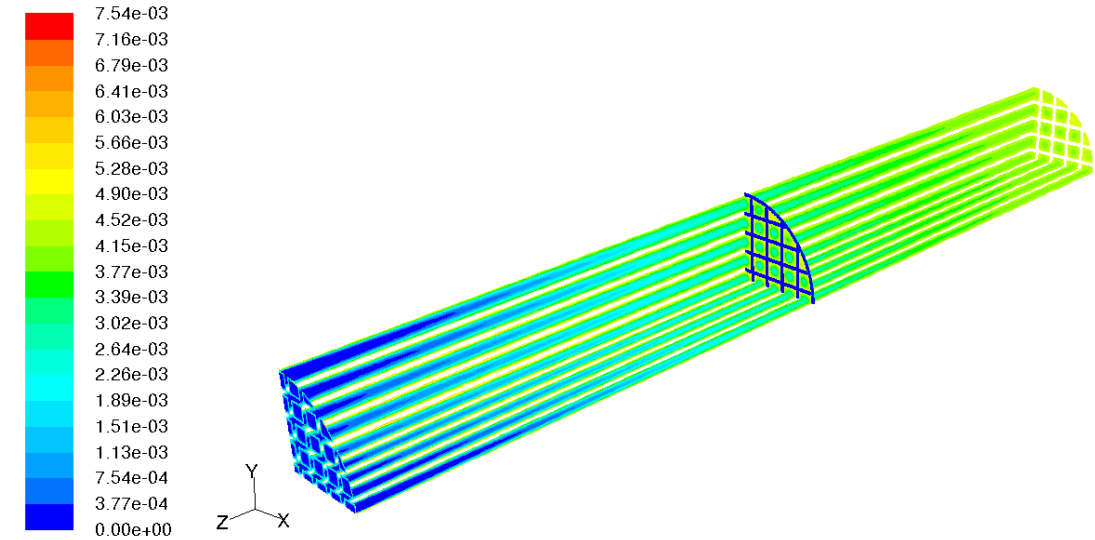

Figure 4.12: Contours of molar concentration of H_2 along the length of monolith.

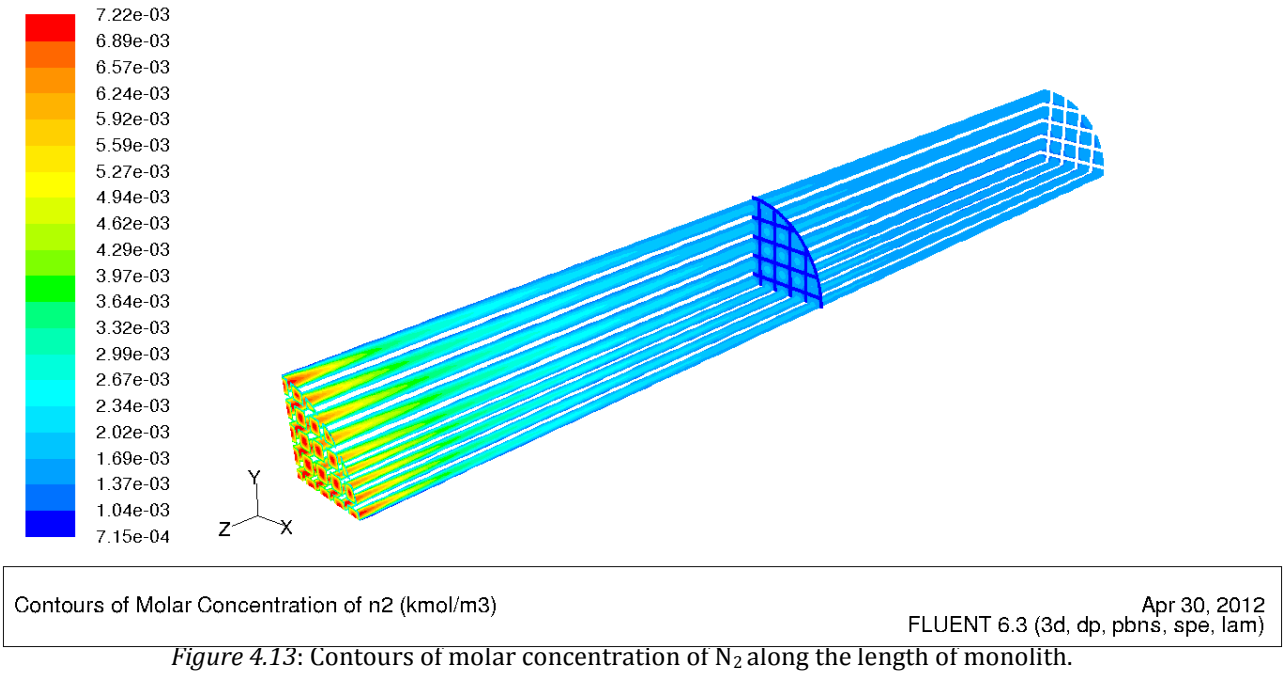

Figure 4.13: Contours of molar concentration of N_2 along the length of monolith.

The averages for CH_4 molar concentration (kgmol/m^3) at inlet and outlet have been computed.

flow_in	0.01113
flow_out	0.001095
Net	0.010035

Hence, Conversion (wrt CH_4) = 0.901586

Chapter 5

CONCLUSIONS

The following conclusions can be drawn about the simulations of reactive flow of monoliths:

1. The results of fluid flow and heat transfer in the base case are similar to those already cited by Mazumdar [43]. Hence the results are validated.
2. Also, because of the simplicity of the geometry, there are no hot spots or fluid recirculation zones formed. All the heat generated by the reactions is carried by the flowing fluids. This is a critical advantage of using a monolith over a packed bed, where flow distribution and heat uniformity depends on the local arrangement of the packings.
3. The reaction mechanism does not have a significant impact on the conversion, as concluded by Mazumdar. The conversion in the case of II-step reaction mechanism is 88.6% whereas in the case of V-step mechanism, it is 90.2%. the error in the conversion values of the two simulations is. These values are compared to the 91% conversion as cited in the literature.

SCOPE FOR FUTURE WORK

The following studies can be performed, in addition, to further analyze the performance of monoliths

1. In this study, only II-step, and V-step reaction mechanisms have been studied that include only the conversion of methane to carbon monoxide. Further reactions can also be added from Raja et al [50] to study side reactions and selectivity.
2. The conversion in a monolith can be compared to that in a catalytic packed bed, to compare the efficiencies in terms of pressure drop, selectivity, and local variations in flow (like stagnation flows, back flows, vortices) and heat transfer uniformities (like hot spots).

REFERENCES

[1] Harris, C.K., Roekaerts, D., Rosendal, F.J.J., Buitendijk, F.G.J., Daskopoulos, Ph., Vreenegoor, A.J.N., & Wang, H. *Computational Fluid dynamics for chemical reactor engineering*. Chem. Engg Sci., **1996**, *1569-1594.*

[2] Lloyd, B., & Boehm, R. Flow and heat transfer around a linear array of spheres. *Numer. Heat Transfer Part A*, **1994**, *237-252*.

[3] Derkx, O.R., & Dixon, A.G. Determination of the fixed bed wall heat transfer coefficient using computational fluid dynamics. *Numer. Heat Transfer Part A*, **1996**, *777-794*.

[4] Logtenberg, S.A., Nijemeisland, M., & Dixon, A.G. Computational fluid dynamics simulations of fluid flow and heat transfer at the wall-particle contact points in a fixed-bed reactor. Chemical Engineering Science, 1999, (54) 2433-2439.

[5] Dixon, A.G., & Nijemeisland, M. CFD as a Design Tool for Fixed-Bed Reactors. *Ind. Eng. Chem. Res.* **2001**, *40, 5246-5254*.

[6] Jakobsen, H.A., Lindborg, H., & Handeland, V. A numerical study of the interactions between viscous flow, transport and kinetics in fixed bed reactors. *Computers and Chemical Engineering,* **2002**, *333–357*

[7] Dixon, A.G., Nijemeisland, M., & Stitt, H. CFD Simulation of Reaction and Heat Transfer near the Wall of a Fixed Bed. *International Journal of Chemical Reactor Engineering*, **2003**, *A22.*

[8] Guardo, A., Coussirat, M., Larrayoz, M.A., Recasens, F., & Egusquiza, E.. CFD Flow and Heat Transfer in Nonregular Packings for Fixed Bed Equipment Design. *Ind. Eng. Chem. Res*. (43) **2004**, *7049-7056.*

[9] Nijemeisland, M., Dixon, A.G., & Stitt, H. Catalyst design by CFD for heat transfer and reaction in steam reforming. *Chemical Engineering Science* (59), **2004**, *5185 – 5191.*

[10] Nijemeisland, M., & Dixon, A.G. CFD Study of Fluid Flow and Wall Heat Transfer in a Fixed Bed of Spheres. *AIChE Journal*, **2004**, *906-921*.

[11] Gunjal, P.R., Ranade, V.V., & Chaudhari, R.V.. Computational Study of a Single-Phase Flow in Packed Beds of Spheres. *AIChE Journal*, **2005**, *365-378*.

[12] Kolaczkowski, S. T., Chao, R., Awdry, S., & Smith, A. Application of A CFD Code (Fluent) To Formulate Models of Catalytic Gas Phase Reactions in Porous Catalyst Pellets. *Trans IChemE, Part A, Chemical Engineering Research and Design*, **2007**, *85(A11): 1539–1552*.

[13] Guardo, A., Coussirat, M., Recasens, F., Larrayoz, M.A., & Escaler, X. CFD studies on particle-to-fluid mass and heat transfer in packed beds: Free convection effects in supercritical fluids. *Chemical Engineering Science*, **2007**, *(62) 5503 – 5511*.

[14] Dixon, A.G, Taskin, M.E., Stitt, E.H., & Nijemeisland M. 3D CFD simulations of steam reforming with resolved intraparticle reaction and gradients. *Chemical Engineering Science*, 2007, (62) 4963 – 4966.

[15] Motlagh, A.H.A., & Hashemabadi, S.H. 3D CFD simulation and experimental validation of particle-to-fluid heat transfer in a randomly packed bed of cylindrical particles. *International Communications in Heat and Mass Transfer,* **2008***, (35) 1183–1189.*

[16] Motlagh, A.H.A., & Hashemabadi, S.H. CFD based evaluation of heat transfer coefficient from cylindrical particles. *International Communications in Heat and Mass Transfer*, **2008**, *(35) 674-680*.

[17] Reddy, R.K., & Joshi, J.B. CFD modeling of pressure drop and drag coefficient in fixed and expanded beds. *Chemical Engineering Research & Design,* **2008***, (86) 444–453*.

[18] Augier, F., Idoux, F., & Delenne, J.Y. Numerical simulations of transfer and transport properties inside packed beds of spherical particles. *Chemical Engineering Science*, **2010**, *(65) 1055–1064*.

[19] Yang, J., Wang, Q., Zeng, M., & Nakayama, A. Computational study of forced convective heat transfer in structured packed beds with spherical or ellipsoidal particles. *Chemical Engineering Science*, **2010**, *(65) 726–738*.

[20] Reddy, R.K., & Joshi, J.B. CFD modeling of pressure drop and drag coefficient in fixed beds: Wall effects. *Particuology*, **2010**, *(8) 37–43*.

[21] Dixon, A.G, Taskin, M.E., Stitt, E.H., & Nijemeisland M. CFD Method to Couple Three-Dimensional Transport and Reaction inside Catalyst Particles to the Fixed Bed Flow Field*. Ind. Eng. Chem. Res.* **2010**, *49, 9012–9025*.

[22] Dixon, A.G, Taskin, M.E., Stitt, E.H., & Nijemeisland M. Systematic mesh development for 3D CFD simulation of fixed beds: Single sphere study. *Computers and Chemical Engineering* **2011**, *35, 1171–1185.*

[23] Valluri, P., Matar, O.K., Hewitt, G.F., & Mendes, M.A. Thin film flowover structured packings at moderate Reynolds numbers. *Chemical Engineering Science* **2005***, 60, 1965 – 1975*.

[24] Petre, C.F., Larachi, F., Iliuta, I., & Grandjean, B.P.A. Pressure drop through structured packings: Breakdown into the contributing mechanisms by CFD modeling. *Chemical Engineering Science* **2003**, *(58),163 – 177*.

[25] Gu, F., Liu, C.J., Yuan, X.G., & Yu, G.C. CFD Simulation of Liquid Film Flow on Inclined Plates. *Chem.Eng. Technol.* **2004**, *(27), 1099-1104.*

[26] Said, W., Nemer, M., & Clodic, D. Modeling of dry pressure drop for fully developed gas flow in structured packing using CFD simulations. *Chemical Engineering Science* **2011**, *(66), 2107–2117.*

[27] Nikou, M.R.K., & Ehsani, M.R. Turbulence models application on CFD simulation of hydrodynamics, heat and mass transfer in a structured packing. *International Communications in Heat and Mass Transfer* **2008,** *(35), 1211–1219*.

[28] Fernandes, J., Simões, P.C., Mota, J.P.B., & Saatdjian, E. Application of CFD in the study of supercritical fluid extraction with structured packing: Dry pressure drop calculations. *J. of Supercritical Fluids* **2008***,(47), 17–24*.

[29] Fernandes, J., Lisboa, P.F., Simões, P.C., Mota, J.P.B., & Saatdjian, E. Application of CFD in the study of supercritical fluid extraction with structured packing:Wet pressure drop calculations. *J. of Supercritical Fluids* **2009**, *(50), 61-68*.

[30] Mahr, B., & Mewes, D. CFD Modelling and Calculation of Dynamic Two-Phase Flow in Columns Equipped with Structured Packing. *Chemical Engineering Research and Design* **2007**, *1112-1122*.

[31] Zivdar, M., Rahimi, R., Nasr, M., & Haghshenasfard, M. CFD Simulations of Pressure Drop in KATAPAK-S Structured packing. *Iranian Journal of Chemical Engineering* **2005**, *64-71*.

[32] Bessou, V., Rouzineau, D., Pre´vost, M., Abbe´, F., Dumont, C., Maumus, J.P., & Meyer, M. Performance characteristics of a new structured packing. *Chemical Engineering Science* **2010***, (65), 4855–4865.*

[33] Wen, X., Afacan, A., Nandakumar, K., & Chuang, K.T. Development of a Novel Vertical-Sheet Structured Packing. *Chemical Engineering Research and Design* **2005**, *83(A5): 515–526*.

[34] Szulczewska, B., Zbicinski, I., & Gorak, A. Liquid Flow on Structured Packing: CFD Simulation and Experimental Study. *Chem. Eng. Technol*. **2003**, *(26), 580-584*.

[35] Lui, H., Zhao, J., Li, C., & Li, S. Conceptual design and CFD simulation of a novel metal-based monolith reactor with enhanced mass transfer. *Catalysis Today* **2005**, *105, 401–406*.

[36] Benedetto, A.D., Marra, F.S., & Russo, G. Heat and mass fluxes in presence of superficial reaction in a not completely developed laminar flow. *Chemical Engineering Science,* **2003***, 58, 1079 – 1086.*

[37] Canu, P., & Vecchi, S. CFD Simulation of Reactive Flows: Catalytic Combustion in a Monolith. *AIChE Journal* **2002**, *48, 2921-2935*.

[38] Donsı, F., Benedetto, A.D., Marra, F.S., & Russo, G. Effect of the Re number on heat and mass transport in a catalytic monolith. *Catalysis Today* **2006**, *117, 498–505*.

[39] Mei H., Li, C., Ji, S., & Liu, H. Modeling of a metal monolith catalytic reactor for methane steam reforming–combustion coupling. *Chemical Engineering Science* **2007**, 62, 4*294 – 4303.*

[40] Perdana, I., Creasera, D., Bendiyasab, I.M., & Tyosob, B.W. Modelling NOx adsorption in a thin NaZSM-5 film supported on a cordierite monolith. *Chemical Engineering Science* **2007**, *62, 3882 – 3893*.

[41] Chen, J., Yang, H., Wang, N., Ring, Z., & Dabros, T. Mathematical modeling of monolith catalysts and reactors for gas phase reactions. *Applied Catalysis A: General* **2008,** *345, 1–11.*

[42] Lei, Z., Liu, X., & Jia, M. Modeling of Selective Catalytic Reduction (SCR) for NO Removal Using Monolithic Honeycomb Catalyst. *Energy Fuels* **2009***, 23, 6146 – 6151*.

[43] Kumar, A., & Mazumder, S. Toward simulation of full-scale monolithic catalytic converters with complex heterogeneous chemistry. Computers and Chemical Engineering **2010**, 34, 135–145.

[44] Kumar, A., & Mazumder, S. Adaptation and application of the in situ Adaptive Tabulation (ISAT) procedure to reacting flow calculations with complex surface chemistry. *Computers and Chemical Engineering* **2011***, 35, 1317–1327.*

[45] Grimm, M., & Mazumder, S. Numerical investigation of wall heat conduction effects on catalytic combustion in split and continuous monolith tubes. *Computers and Chemical Engineering* **2008**, *32, 552–560.*

[46] Lynch, C. T. (Ed.). (1975). CRC handbook of material science, Vol. III. Non-metallic materials and applications. Boca Raton, FL: CRC Press.

[47] Mohammad, I., Asghar, A., Nakhaei, P.A., Nasibeh, H., & Morteza, A. CFD modeling of hydrogen production using steam reforming of methane in monolith reactors: Surface or volume-base reaction model?. *Internation Journal of Hydrogen Energy,* **2011***, 36, 15602-15610.*

[48] Fluent 6.3 Help Manual

[49] http://www.cfd-online.com/Forums

[50] Raja, L.L., Kee, R.J., Deutschmann O., Warnatz,J., & Schmidt, L.D. A critical evaluation of Navier–Stokes, boundary-layer, and plug-flow models of the flow and chemistry in a catalytic-combustion monolith. *Catalysis Today,* **2009**, *59, 47–60.*